Rapid Communications

Topological phase transition between distinct Weyl semimetal states in $MoTe_2$

Anmin Zhang,[1,2,*] Xiaoli Ma,[2,*] Changle Liu,[2] Rui Lou,[2] Yimeng Wang,[2] Qiaohe Yu,[2] Yiyan Wang,[2] Tian-long Xia,[2] Shancai Wang,[2] Lei Zhang,[3] Xiaoqun Wang,[4] Changfeng Chen,[5] and Qingming Zhang[2,6,1,†]

[1]*School of Physical Science and Technology, Lanzhou University, Lanzhou 730000, China*

[2]*Department of Physics, Renmin University of China, Beijing 100872, China*

[3]*Anhui Key Laboratory of Condensed Matter Physics at Extreme Conditions, High Magnetic Field Laboratory, Chinese Academy of Sciences, Hefei 230031, China*

[4]*Key Laboratory of Artificial Structures and Quantum Control (Ministry of Education), School of Physics and Astronomy, Tsung-Dao Lee Institute, Shanghai Jiao Tong University, Shanghai 200240, China*

[5]*Department of Physics and Astronomy, University of Nevada, Las Vegas, Nevada 89154, USA*

[6]*Beijing National Laboratory for Condensed Matter Physics, Institute of Physics, Chinese Academy of Sciences, Beijing 100190, China*

(Received 17 April 2018; revised manuscript received 9 November 2019; published 25 November 2019)

We present experimental evidence of an intriguing phase transition between distinct topological states in the type-II Weyl semimetal $MoTe_2$. We observe anomalies in the Raman phonon frequencies and linewidths as well as electronic quasielastic peaks around 70 K, which, together with structural, thermodynamic measurements, and electron-phonon coupling calculations, demonstrate a temperature-induced transition between two topological phases previously identified by contrasting spectroscopic measurements. An analysis of experimental data suggests electron-phonon coupling as the main driving mechanism for the change of key topological characters in the electronic structure of $MoTe_2$. We also find the phase transition to be sensitive to sample conditions distinguished by synthesis methods. These discoveries of temperature and material condition-dependent topological phase evolutions and transitions in $MoTe_2$ advance the fundamental understanding of the underlying physics and enable an effective approach to tuning Weyl semimetal states for technological applications.

DOI: 10.1103/PhysRevB.100.201107

Recent years have seen the dramatic rise of a new class of quantum materials whose electronic states exhibit symmetry protected topological orders [1,2]. Such electronic states are insensitive to local decoherence processes, thus offering great promise for constructing quantum computing and high-speed electronic and spintronics devices. Distinct topological states, such as topological insulators, Dirac semimetals, and type-I and type-II Weyl semimetals, have been theoretically [1–8] proposed and experimentally [9–18] realized in real materials. A central task in this research field is to unravel the material and environment (e.g., pressure, temperature, etc.) conditions conducive to the existence of topologically ordered phases. To this end, it is essential to be able to induce and control the phase transition that allows an effective manipulation of the unique properties of the topological states. Significant progress has been made in understanding the transitions between topologically trivial and nontrivial states. Recent theoretical studies have shown that strain [19,20], phonon [21,22], and/or disorder [23] can induce topological phase transitions that greatly influence electronic states and properties. For instance, when a topological transition occurs, topological surface states dramatically change [8–13], greatly impacting transport behaviors [15–18,24], and phonon modes strongly coupled to electrons may also behave anomalously [25,26]. A recent experiment revealed that a structural transition can act as a switch of the topological phase transition [27]. Meanwhile, however, transitions between distinct topologically ordered states have remained largely unexplored, especially on the experimental front.

Molybdenum ditelluride ($MoTe_2$), a type-II Weyl semimetal (WSM) [19,20,28], offers an excellent platform to probe distinct topological phases and possible transitions among them. $MoTe_2$ has three structural phases: $2H$ (hexagonal, space group $P63/mmc$), $1T'$ (monoclinic, $P21/m$), and T_d (orthorhombic, $Pnm21$) [29]. Topological surface states have been observed in T_d-$MoTe_2$ at low temperatures [30–35]. Angle-resolved photoemission (ARPES) measurements [33] suggested that a $MoTe_2$ specimen grown by a flux method harbors an electronic structure containing four Weyl points (WPs), and this conclusion was supported by electronic band calculations [20]. On the other hand, contrasting ARPES experiments [34,35] observed eight WPs in $MoTe_2$ grown by a chemical vapor transport method, and the results are also supported by calculations [19,35]. The diverging theoretical results likely stem from using the different lattice constants measured at different temperatures [19,20], while the variation of the experimental results suggests that the nature of the topological states are highly sensitive to sample conditions. These results imply that a topological phase transition may occur in $MoTe_2$ [19,20], but experimental evidence is still lacking. The objective of our present Rapid Communication is to seek and establish clear experimental signatures of the transition between distinct Weyl semimetal phases, thus unifying the seemingly inconsistent ARPES results and

*These authors contributed equally to this work.
†qmzhang@ruc.edu.cn

resolving the nature of the topological states in $MoTe_2$, which is crucial to understanding the fundamental physics of these topological quantum materials and their exotic properties, such as topological superconductivity [36–43].

In this Rapid Communication, we examine the topological states in $MoTe_2$ by performing Raman scattering, structural, and thermodynamic measurements on crystals grown using different synthesis methods (the crystal-growth and measurement methods can be found in the Supplemental Material [44]). Our results reveal that several phonon modes show strong electron-phonon coupling (EPC) effects. The frequencies, widths, and q factors of these phonon modes exhibit clear anomalies at ~70 K in $MoTe_2$ crystals grown by a flux method (hereafter referred to as flux $MoTe_2$), but, surprisingly, not in the crystals grown by a chemical vapor transport method (CVT $MoTe_2$). The intensities of the low-frequency quasielastic peak (QEP), originating from the electronic Raman response, also show a minimum at 70 K in flux $MoTe_2$ but not in CVT $MoTe_2$. These anomalies are further corroborated by our transport measurements. All these observations, together with EPC calculations, establish a clear case of sample-dependent topological characters of the electronic structure and an intriguing phase transition in flux $MoTe_2$ between distinct Weyl semimetal states. Raman scattering results, together with x-ray diffraction (XRD), transport, specific heat data, and EPC calculations, consistently demonstrate that the transition is an electronic/topological phase transition driven by the strong EPC effect. These results lead to a phase diagram that helps distinguish different topological ground states of $MoTe_2$ under different material and temperature conditions.

Low-temperature T_d-$MoTe_2$ hosts 33 Raman modes, among which 17 modes visible on the *ab* plane have been well assigned [45–48]. Here, we focus on the modes with stronger intensities. These modes can be divided into two groups: those with symmetric peak profiles [Figs. 1(a) and 1(b)], and others with asymmetric profiles [Figs. 1(g) and 1(h)]. The temperature evolution of the $^2A_1$ and $^2A_2$ modes, which are the vibrations dominated by Te atoms along the b and a axes, respectively [45], is shown in Figs. 1(a) and 1(b). In Figs. 1(c)–1(f), we show the temperature dependence of their frequencies and linewidths extracted by a Lorentzian fitting (an example of fitting is shown in Supplemental Material, Fig. S1 [44]).

The $^2A_1$ mode exhibits an unusual softening in frequency and broadening in width with decreasing temperature [Figs. 1(c) and 1(d)]. This is in stark contrast to the normal hardening and narrowing of the $^2A_2$ mode related to the anharmonic phonon coupling [49] [Figs. 1(e) and 1(f)], and can be attributed to the EPC (see the Supplemental Material, Secs. III and X [44]). Consistently, the anomalous broadening in linewidth can be also well understood within the EPC picture [Fig. 1(d)]. In the EPC theory [50], the real part of the self-energy represents the frequency shift and the imaginary part gives the phonon broadening due to its interaction with the electronic continuum. Both parts are driven toward constant values by the Fermi-Dirac distribution function approaching zero temperature, as seen in CVT $MoTe_2$ [Figs. 1(c) and 1(d)]. Surprisingly, the flux $MoTe_2$ follows a softening tendency at higher temperatures but upon cooling exhibits a dramatic upturn at $T_t \sim 70$ K [Figs. 1(c) and 1(d)]. This

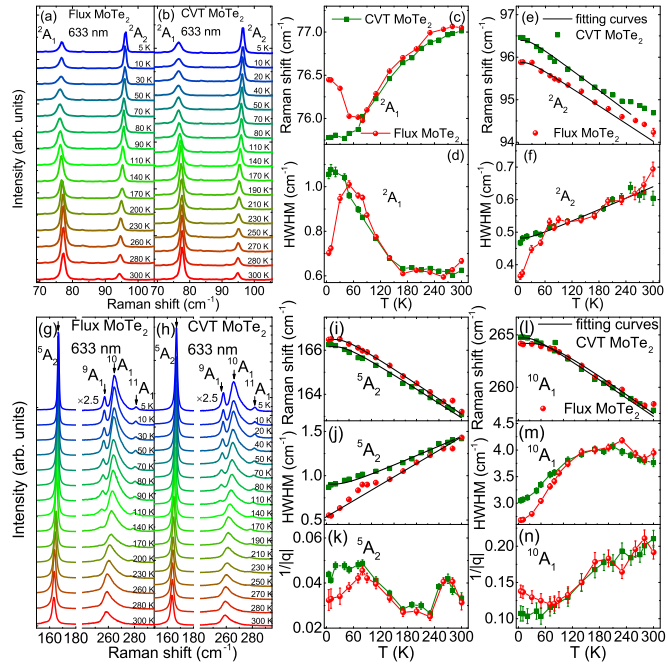

FIG. 1. Anomalies in phonon Raman spectra. (a), (b), (g), and (h) Temperature evolution of the $^2A_1$, $^2A_2$, $^5A_2$, and $^{10}A_1$ modes in flux $MoTe_2$ and CVT $MoTe_2$. (c)–(f), (i)–(n) Temperature dependence of peak positions, linewidths, and asymmetry factor q of these phonon modes.

anomalous behavior clearly signals changes in the underlying phonon or electronic structures.

The temperature evolution of the asymmetric $^5A_2$ and $^{10}A_1$ modes is presented in Figs. 1(g) and 1(h). In the phonon softening picture, this asymmetry reflects the EPC described by the Fano formula [50]. The parameters by Fano fitting and their temperature dependence are summarized in Figs. 1(i)–1(n) (the fitting details are shown in Supplemental Material, Fig. S1 [44]).

For the $^5A_2$ and $^{10}A_1$ modes, the anomalies in linewidth and $1/|q|$ at ~70 K can be clearly seen in flux $MoTe_2$ but not in CVT $MoTe_2$. The anomalies unambiguously point to a phase transition in flux $MoTe_2$. In other words, flux $MoTe_2$ and CVT $MoTe_2$ share the same phase at high temperatures, but fall into different phases below 70 K. The observation that there is no anomaly in the lattice constant and/or specific heat at the transition temperature [Fig. 3(c)] suggests that this phase transition is not driven by structural changes (see below for further discussions). We have repeated Raman scattering measurements on different batches of crystals, and the results show perfect repeatability (see Supplemental Material, Fig. S3 [44]).

The phase transition at 70 K is further evidenced by electronic Raman response (ERS), which is an inelastic light scattering process by band electrons and includes the influence of low-energy single-particle excitations and high-energy collective plasmon excitations. The transferred energies in this process would be very small if the involved photons and band electrons have small momenta and small Fermi velocities, respectively. In such a case, electronic Raman scattering manifests itself as a quasielastic peak (QEP) [51]. The

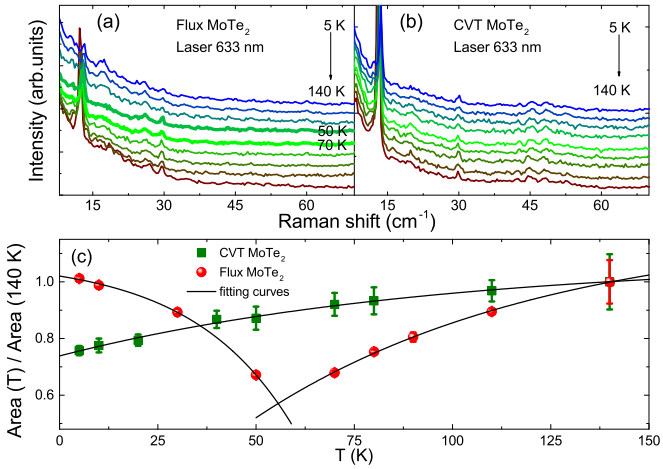

FIG. 2. Anomalies in quasielastic peaks at low wave numbers. (a), (b) Low-frequency quasielastic peaks at various temperatures in flux $MoTe_2$ and CVT $MoTe_2$. (c) Temperature dependence of the normalized intensities of quasielastic peaks. Black lines in (c) are fitted using the exponential functions ($I = I_0 + I_1 e^{\frac{-T}{\tau}}$ where I_0, I_1, τ are parameters). The phonons below 15 cm^{-1} are the shear mode [46] with A_1 symmetry. So the intensities are strongly affected by the angle between the polarization of the incident light and the crystallographic axis. The shear mode shows different intensities in (a) and (b) for the different angles.

low-energy QEPs can be clearly seen in both the flux and CVT $MoTe_2$ samples [Figs. 2(a) and 2(b)]. However, the temperature dependences of QEPs are very different for the two samples. In CVT $MoTe_2$, the QEP intensity monotonously declines with decreasing temperature and smoothly passes through the transition temperature; meanwhile, the QEP in flux $MoTe_2$ exhibits a clear minimum at $T_t \approx 70$ K. This difference suggests two distinct phases at low temperatures for the two samples, in agreement with the findings from the phonon spectra, and the anomaly in QEP points to a phase transition of the electronic states since QEP is contributed

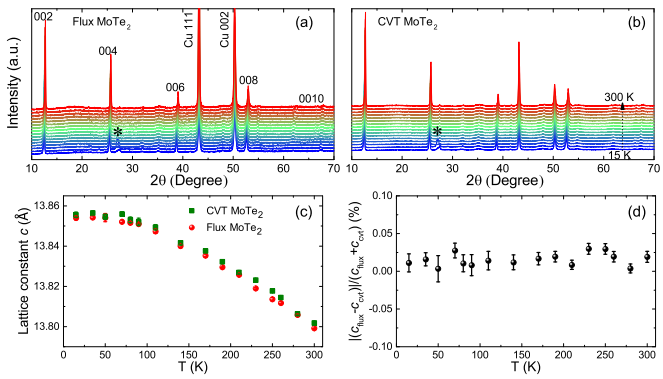

FIG. 3. Nearly identical structural parameters in two samples. (a), (b) XRD patterns at various temperatures in flux $MoTe_2$ and CVT $MoTe_2$. (c) Temperature dependence of lattice constant c. (d) Relative differences of c between two samples at various temperatures, which remain less than 0.05% at all temperatures. The broad peaks at low temperatures marked by * in (a) and (b) are instrumental signals (see Supplemental Material, Fig. S6 [44]).

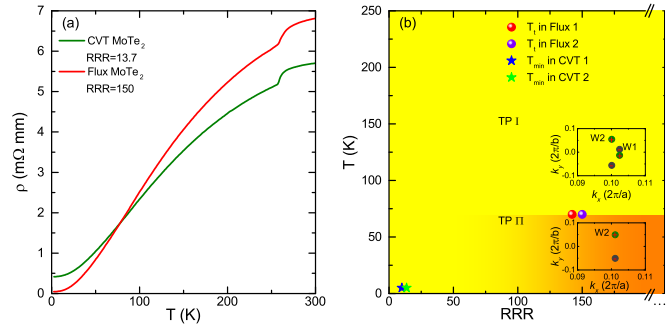

FIG. 4. R-T curves and T-RRR phase diagram. (a) R-T curves of a flux $MoTe_2$ and a CVT $MoTe_2$. (b) Temperature-RRR phase diagram of $MoTe_2$. In the low-RRR region, the star symbols denote the data points taken on two CVT $MoTe_2$ samples at the lowest temperature ($T_{min} = 5$ K) in our measurements, where no signs of a temperature-induced phase transition have been detected. In the high-RRR region, the sphere symbols denote the transition temperatures (T_t) given by the phonon Raman spectra obtained on two flux $MoTe_2$ samples. The insets in (b) are schematic band structures in the two topological phases [19,20].

purely by electrons. This assessment is further supported by our transport measurements. We extracted electronic concentration n_e and the mobilities of both electrons and holes from the two-carrier model analysis of magnetoresistivity ρ_{xx} and Hall resistivity ρ_{xy}. The results show a sharp upturn below 70 K in flux $MoTe_2$ but smoothly evolve with temperature in CVT $MoTe_2$ (Supplemental Material, Fig. S4 [44]). This observation confirms the phase transition of the electronic states in flux $MoTe_2$.

To assess the origin of the phase transition, we further performed XRD measurements on the two samples. The XRD patterns at various temperatures are shown in Figs. 3(a) and 3(b). The preferred-orientation effect of layered materials makes the ($00L$) peaks much stronger than others. The extracted lattice constants [Fig. 3(c)] indicate that $MoTe_2$ shows a negative thermal expansion along the c axis, in agreement with previous studies [35]. The lattice constant c has a smooth temperature evolution and tends to be saturated below 100 K. This result supports the conclusion that the softening of the $^2A_1$ mode and the anomalies around T_t are not related to any structural change. The relative difference of c between the two samples is negligibly small at less than 0.05% at all temperatures [Fig. 3(d)]. Thus, we can conclude that the phase transition at 70 K in flux $MoTe_2$ is an electronic phase transition rather than a structural one, which is corroborated by the absence of any anomaly around T_t in the specific heat of flux $MoTe_2$ (Supplemental Material, Fig. S2 [44]). All these results point to the conclusion that an electronic topological phase transition occurs in flux $MoTe_2$ but not in CVT $MoTe_2$.

To further characterize the material dependence of the topological phase transition in $MoTe_2$, we have measured the resistivity as a function of temperature from 2.5 to 300 K on two batches of $MoTe_2$ crystals, two synthesized using the flux method and two using the CVT method [Fig. 4(a) and Supplemental Material, Fig. S5 [44]]. Remarkably, the residual resistivity ratio (RRR), defined as the ratio of resistivity values at room temperature (300 K) and in the

low-temperature limit, of flux $MoTe_2$ is an order of magnitude larger than that of CVT $MoTe_2$. Such a large disparity in RRR, also reported in previous studies [30,31,36–39,52,53], implies some degree of disorder or inhomogeneity in CVT $MoTe_2$. From our sample- and temperature-dependent data, we have constructed a phase diagram in the T-RRR phase space for the two topological phases [Fig. 4(b)], containing eight and four WPs, respectively, which have been observed in separate ARPES measurements in the $MoTe_2$ crystals grown by CVT and flux methods [30–35]. Our Raman data are consistent with the ARPES observations as illustrated in the T-RRR phase diagram, where the phase at higher temperatures is in one topological state (TP I, 8-WP), while the phase in the high-RRR and low-temperature region is in another topological state (TP II, 4-WP). Our results show that upon cooling the high-RRR flux $MoTe_2$ sample undergoes a transition from the TP I to TP II Weyl semimetal state; meanwhile, the low-RRR CVT $MoTe_2$ sample remains in the TP I state throughout the entire temperature range. These results explain the previously reported divergent topological characters observed in different $MoTe_2$ crystals [19,20,33–36]. The sample-sensitive temperature-induced transition highlights the material (RRR) and environment (temperature) dependence of the topological state in $MoTe_2$. Further studies are required to map out the full phase boundary between the TP I and TP II states; one may also establish phase diagrams in other material and environment parameter spaces.

The key topological character of a Weyl semimetal is the nodal structure of its electronic bands, where the twofold degenerate bands cross with a linear dispersion. The number and distribution of such Weyl points (WPs) define the topological properties crucial to the fundamental understanding and practical applications of these materials. The WPs in $MoTe_2$ are generally divided into two groups, namely, W1 WPs that are closely positioned in the momentum space and W2 WPs that are well separated. It was shown theoretically that a strain of 0.1% along the a axis of $MoTe_2$ can tune the appearance of W1 WPs [20]. According to the temperature dependence of the lattice constant a, a temperature change over 70 K (from 0 K to T_t) would induce a strain over 0.1% in $MoTe_2$ [35], making a topological phase transition induced by the thermal expansion plausible. Our experiments show, however, that the lattice constants of flux $MoTe_2$ and CVT $MoTe_2$ remain very close (less than 0.05% difference) in the entire studied temperature range, yet the transition only occurs in the flux samples. This result rules out the change in the lattice constant as the origin of the observed topological phase transition. Meanwhile, the temperature influence on E_F may trigger a Lifshitz transition. However, it has been shown that a temperature change from 0 K to T_t (70 K) is too small to bring about an observable modification in E_F sufficient to drive a topological transition in $MoTe_2$ [52], while the change in the ratio between the hole and electron densities (n_h/n_e) near T_t [39,52] may reflect the reconstruction of the Fermi surface induced by the topological transition. Finally, a strong EPC in $MoTe_2$ has been revealed in our experiments. The EPC can simultaneously alter the phononic energy and lifetime and the electronic structure. A topological transition induced by EPC has been theoretically studied [21,22]. In our Rapid Communication, we also made the EPC calculation (see details in Supplemental Material [44], Sec. X), which shows that the EPC contribution to the electronic self-energy generally increases with temperature because of the fast rising in the phonon occupation number, and the EPC-induced changes in the electronic structure could close the small gap between two bands, which eventually cross and form W1 WPs, causing a topological phase transition from one phase (TP II) hosting four WPs to another phase (TP I) containing eight WPs. When the topological phase transition occurs, the phonon linewidth reverses as well. This behavior can serve as a good indicator of electronic band inversions [26], thus explaining the anomaly of the linewidths of the $^2A_1$ mode observed in $MoTe_2$.

Our results indicate a transition of the topological ground state from the TP I phase with eight WPs at temperatures above 70 K to the TP II phase with four WPs at lower temperatures in the high-RRR flux $MoTe_2$ crystals. Meanwhile, the low-RRR CVT $MoTe_2$ remains in the TP I phase in the entire temperature region from 300 K down to 5 K, which is lower than in recent ARPES experiments (10 and 6–20 K) [34,35]. This suggests that disorder may have caused substantial changes in the topological ground state of CVT $MoTe_2$ by modifying the electronic self-energies [23]. It indicates that the EPC in CVT $MoTe_2$ is significantly overcome by the disorder effect and can no longer induce a topological phase transition (TP II to TP I) as observed in flux $MoTe_2$. These contrasting results raise important questions about the fundamental interactions in $MoTe_2$.

We have shown Raman, structural, and transport measurements that demonstrate a temperature-induced electronic transition in flux $MoTe_2$ and the EPC calculation indicates this transition is a topological phase transition between distinct Weyl semimetal states. These results, combined with our and existing ARPES data, identify a topological ground-state transition from a TP I phase hosting eight WPs at temperatures above 70 K to a TP II phase containing four WPs at lower temperatures. Our study also shows that $MoTe_2$ crystals obtained by a chemical vapor transport method remain in the TP I phase down to 5 K without any sign of a phase transition. Based on these findings, we have constructed a temperature-RRR phase diagram that reconciles the divergent views on the topological characters of the electronic structure of $MoTe_2$. The present results have broad implications for major topological properties such as the Fermi arc surface structures and transport behaviors; they also raise fundamental questions on the roles of the key physical processes and material conditions in determining the properties of topological materials. Our experiments and calculation suggest strong EPC in $MoTe_2$ as the driving mechanism for the observed topological phase transition, highlighting a major influence of EPC effects in topological materials. Our results also indicate that disorder may have a significant role in impeding a topological phase transition in CVT $MoTe_2$. These insights advance and enrich the fundamental understanding of Weyl semimetals and pave the way for further research to unveil other physics in this class of materials.

We thank Shanshan Sun for assisting with specific heat measurements. This work was supported by the Ministry of Science and Technology of China (2016YFA0300504,

2017YFA0302904, and 2016YFA0300501) and the NSF of China (11604383, 11774419, 11474357, 11574391, 11574200, and 11974244). A.Z. and T.-l.X. were supported by the Fundamental Research Funds for the Central Universities and the Research Funds of Renmin University of China (18XNLG23 and 14XNLQ07).

[1] M. Z. Hasan and C. L. Kane, Rev. Mod. Phys. **82**, 3045 (2010).
[2] X.-L. Qi and S.-C. Zhang, Rev. Mod. Phys. **83**, 1057 (2011).
[3] X. G. Wan, A. M. Turner, A. Vishwanath, and S. Y. Savrasov, Phys. Rev. B **83**, 205101 (2011).
[4] G. Xu, H. Weng, Z. Wang, X. Dai, and Z. Fang, Phys. Rev. Lett. **107**, 186806 (2011).
[5] H. M. Weng, C. Fang, Z. Fang, B. A. Bernevig, and X. Dai, Phys. Rev. X **5**, 011029 (2015).
[6] H. B. Nielsen and M. Ninomiya, Nucl. Phys. B **185**, 20 (1981).
[7] H. B. Nielsen and M. Ninomiya, Phys. Lett. B **130**, 389 (1983).
[8] A. A. Soluyanov, D. Gresch, Z. Wang, Q. S. Wu, M. Troyer, X. Dai, and B. A. Bernevig, Nature (London) **527**, 495 (2015).
[9] S.-Y. Xu, I. Belopolski, N. Alidoust, M. Neupane, G. Bian, C. Zhang, R. Sankar, G. Chang, Z. Yuan, C.-C. Lee, S.-M. Huang, H. Zheng, J. Ma, D. S. Sanchez, B. Wang, A. Bansil, F. Chou, P. P. Shibayev, H. Lin, S. Jia, and M. Z. Hasan, Science **349**, 613 (2015).
[10] B. Q. Lv, H. M. Weng, B. B. Fu, X. P. Wang, H. Miao, J. Ma, P. Richard, X. C. Huang, L. X. Zhao, G. F. Chen, Z. Fang, X. Dai, T. Qian, and H. Ding, Phys. Rev. X **5**, 031013 (2015).
[11] L. X. Yang, Z. K. Liu, Y. Sun, H. Peng, H. F. Yang, T. Zhang, B. Zhou, Y. Zhang, Y. F. Guo, M. Rahn, D. Prabhakaran, Z. Hussain, S.-K. Mo, C. Felser, B. Yan, and Y. L. Chen, Nat. Phys. **11**, 728 (2015).
[12] B. Q. Lv, N. Xu, H. M. Weng, J. Z. Ma, P. Richard, X. C. Huang, L. X. Zhao, G. F. Chen, C. Matt, F. Bisti, V. Strokov, J. Mesot, Z. Fang, X. Dai, T. Qian, M. Shi, and H. Ding, Nat. Phys. **11**, 724 (2015).
[13] S.-Y. Xu, N. Alidoust, I. Belopolski, Z. Yuan, G. Bian, T.-R. Chang, H. Zheng, V. N. Strocov, D. S. Sanchez, G. Chang, C. Zhang, D. Mou, Y. Wu, L. Huang, C.-C. Lee, S.-M. Huang, B. Wang, A. Bansil, H.-T. Jeng, T. Neupert, A. Kaminski, H. Lin, S. Jia, and M. Z. Hasan, Nat. Phys. **11**, 748 (2015).
[14] N. Xu, H. M. Weng, B. Q. Lv, C. Matt, J. Park, F. Bisti, V. N. Strocov, D. Gawryluk, E. Pomjakushina, K. Conder, N. C. Plumb, M. Radovic, G. Autès, O. V. Yazyev, Z. Fang, X. Dai, G. Aeppli, T. Qian, J. Mesot, H. Ding, and M. Shi, Nat. Commun. **7**, 11006 (2016).
[15] C. Zhang, S.-Y. Xu, I. Belopolski, Z. Yuan, Z. Lin, B. Tong, N. Alidoust, C.-C. Lee, S.-M. Huang, H. Lin, M. Neupane, D. S. Sanchez, H. Zheng, G. Bian, J. Wang, C. Zhang, T. Neupert, M. Z. Hasan, and S. Jia, Nat. Commun. **7**, 10735 (2016).
[16] X. Huang, L. Zhao, Y. Long, P. Wang, D. Chen, Z. Yang, H. Liang, M. Xue, H. Weng, Z. Fang, X. Dai, and G. Chen, Phys. Rev. X **5**, 031023 (2015).
[17] C. Shekhar, F. Arnold, S.-C. Wu, Y. Sun, M. Schmidt, N. Kumar, A. G. Grushin, J. H. Bardarson, R. Donizeth dos Reis, M. Naumann, M. Baenitz, H. Borrmann, M. Nicklas, E. Hassinger, C. Felser, and B. Yan, Nat. Commun. **7**, 11615 (2016).
[18] X. Yang, Y. Liu, Z. Wang, Y. Zheng, and Z.-A. Xu, arXiv:1506.03190.
[19] Y. Sun, S.-C. Wu, M. N. Ali, C. Felser, and B. Yan, Phys. Rev. B **92**, 161107(R) (2015).
[20] Z. Wang, D. Gresch, A. A. Soluyanov, W. Xie, S. Kushwaha, X. Dai, M. Troyer, R. J. Cava, and B. A. Bernevig, Phys. Rev. Lett. **117**, 056805 (2016).
[21] I. Garate, Phys. Rev. Lett. **110**, 046402 (2013).
[22] K. Saha and I. Garate, Phys. Rev. B **89**, 205103 (2014).
[23] M. J. Park, B. Basa, and M. J. Gilbert, Phys. Rev. B **95**, 094201 (2017).
[24] Z.-M. Yu, Y. Yao, and S. A. Yang, Phys. Rev. Lett. **117**, 077202 (2016).
[25] A. Sharafeev, V. Gnezdilov, R. Sankar, F. C. Chou, and P. Lemmens, Phys. Rev. B **95**, 235148 (2017).
[26] K. Saha, K. Légaré, and I. Garate, Phys. Rev. Lett. **115**, 176405 (2015).
[27] A. N. Berger, E. Andrade, A. Kerelsky, D. Edelberg, J. Li, Z. Wang, L. Zhang, J. Kim, N. Zaki, J. Avila, C. Chen, M. C. Asensio, S.-W. Cheong, B. A. Bernevig, and A. N. Pasupathy, npj Quantum Mater. **3**, 2 (2018).
[28] T.-R. Chang, S.-Y. Xu, G. Chang, C.-C. Lee, S.-M. Huang, B. Wang, G. Bian, H. Zheng, D. S. Sanchez, I. Belopolski, N. Alidoust, M. Neupane, A. Bansil, H.-T. Jeng, H. Lin, and M. Zahid Hasan, Nat. Commun. **7**, 10639 (2016).
[29] R. Clarke, E. Marseglia, and H. P. Hughes, Philos. Mag. B **38**, 121 (1978).
[30] L. Huang, T. M. McCormick, M. Ochi, M.-T. Suzuki, R. Arita, Y. Wu, D. Mou, H. Cao, J. Yan, N. Trivedi, and A. Kaminski, Nat. Mater. **15**, 1155 (2016).
[31] K. Deng, G. Wan, P. Deng, K. Zhang, S. Ding, E. Wang, M. Yan, H. Huang, H. Zhang, Z. Xu, J. Denlinger, A. Fedorov, H. Yang, W. Duan, H. Yao, Y. Wu, Y. Shoushan Fan, H. Zhang, X. Chen, and S. Zhou, Nat. Phys. **12**, 1105 (2016).
[32] A. Liang, J. Huang, S. Nie, Y. Ding, Q. Gao, C. Hu, S. He, Y. Zhang, C. Wang, B. Shen, J. Liu, P. Ai, L. Yu, X. Sun, W. Zhao, S. Lv, D. Liu, C. Li, Y. Zhang, Y. Hu, Y. Xu, L. Zhao, G. Liu, Z. Mao, X. Jia, F. Zhang, S. Zhang, F. Yang, Z. Wang, Q. Peng, H. Weng, X. Dai, Z. Fang, Z. Xu, C. Chen, and X. J. Zhou, arXiv:1604.01706.
[33] N. Xu, Z. J. Wang, A. P. Weber, A. Magrez, P. Bugnon, H. Berger, B. B. Fu, B. Q. Lv, N. C. Plumb, M. Radovic, K. Conder, T. Qian, J. H. Dil, J. Mesot, H. Ding, and M. Shi, arXiv:1604.02116.
[34] J. Jiang, Z. K. Liu, Y. Sun, H. F. Yang, R. Rajamathi, Y. P. Qi, L. X. Yang, C. Chen, H. Peng, C.-C. Hwang, S. Z. Sun, S.-K. Mo, I. Vobornik, J. Fujii, S. S. P. Parkin, C. Felser, B. H. Yan, and Y. L. Chen, Nat. Commun. **8**, 13973 (2017).
[35] A. Tamai, Q. S. Wu, I. Cucchi, F. Y. Bruno, S. Riccò, T. K. Kim, M. Hoesch, C. Barreteau, E. Giannini, C. Besnard, A. A. Soluyanov, and F. Baumberger, Phys. Rev. X **6**, 031021 (2016).
[36] Y. P. Qi, P. G. Naumov, M. N. Ali, C. R. Rajamathi, W. Schnelle, O. Barkalov, M. Hanfland, S. C. Wu, C. Shekhar, Y. Sun, V. Suss, M. Schmidt, U. Schwarz, E. Pippel, P. Werner, R. Hillebrand, T. Forster, E. Kampert, S. Parkin, R. J. Cava,

C. Felser, B. H. Yan, and S. A. Medvedev, Nat. Commun. **7**, 11038 (2016).

[37] F. C. Chen, X. Luo1, R. C. Xiao, W. J. Lu, B. Zhang, H. X. Yang, J. Q. Li, Q. L. Pei, D. F. Shao, R. R. Zhang, L. S. Ling, C. Y. Xi, W. H. Song, Y. P. Sun *et al.*, Appl. Phys. Lett. **108**, 162601 (2016).

[38] H. Takahashi, T. Akiba, K. Imura, T. Shiino, K. Deguchi, N. K. Sato, H. Sakai, M. S. Bahramy, and S. Ishiwata, Phys. Rev. B **95**, 100501(R) (2017).

[39] D. Rhodes, R. Schnemann, N. Aryal, Q. Zhou, Q. R. Zhang, E. Kampert, Y.-C. Chiu, Y. Lai, Y. Shimura, G. T. McCandless, J. Y. Chan, D. W. Paley, J. Lee, A. D. Finke, J. P. C. Ruff, S. Das, E. Manousakis, and L. Balicas, Phys. Rev. B **96**, 165134 (2017).

[40] G. Y. Cho, J. H. Bardarson, Y.-M. Lu, and J. E. Moore, Phys. Rev. B **86**, 214514 (2012).

[41] H. Wei, S.-P. Chao, and V. Aji, Phys. Rev. B **89**, 014506(R) (2014).

[42] G. Bednik, A. A. Zyuzin, and A. A. Burkov, Phys. Rev. B **92**, 035153 (2015).

[43] Z. Guguchia, F. V. Rohr, Z. Shermadini, A. T. Lee, S. Banerjee, A. R. Wieteska, C. A. Marianetti, H. Luetkens, Z. Gong, B. A. Frandsen, S. C. Cheung, C. Baines, A. Shengelaya, A. N. Pasupathy, E. Morenzoni, S. J. L. Billinge, A. Amato, R. J. Cava, R. Khasanov, and Y. J. Uemura, Nat. Commun. **8**, 1082 (2017).

[44] See Supplemental Material at http://link.aps.org/supplemental/10.1103/PhysRevB.100.201107 for details about Raman, structural, transport, and ARPES measurements, and electron-phonon coupling calculations, which includes Refs. [35,53–56].

[45] X. Ma, P. Guo, C. Yi, Q. Yu, A. Zhang, J. Ji, Y. Tian, F. Jin, Y. Wang, K. Liu, T. Xia, Y. Shi, and Q. Zhang, Phys. Rev. B **94**, 214105 (2016).

[46] S. Y. Chen, T. Goldstein, D. Venkataraman, A. Ramasubramaniam, and J. Yan, Nano Lett. **16**, 5852 (2016).

[47] K. Zhang, C. Bao, Q. Gu, X. Ren, H. Zhang, K. Deng, Y. Wu, Y. Li, J. Feng, and S. Zhou, Nat. Commun. **7**, 13552 (2016).

[48] J. Joshi, I. R. Stone, R. Beams, S. Krylyuk, I. Kalish, A. V. Davydov, and P. M. Vora, Appl. Phys. Lett. **109**, 031903 (2016).

[49] M. Balkanski, R. F. Wallis, and E. Haro, Phys. Rev. B **28**, 1928 (1983).

[50] M. Cardona and G. Güntherodt, *Light Scattering in Solids IV* (Springer, New York, 1984), Chap. 2.

[51] B. H. Bairamov, I. P. Ipatova, and V. A. Voitenko, Phys. Rep. **229**, 221 (1993).

[52] F. C. Chen, H. Y. Lv, X. Luo, W. J. Lu, Q. L. Pei, G. T. Lin, Y. Y. Han, X. B. Zhu, W. H. Song, and Y. P. Sun, Phys. Rev. B **94**, 235154 (2016).

[53] Q. Yu, Y. Wang, S. Xu, L. Sun, and T. Xia, Europhys. Lett. **115**, 37007 (2016).

[54] D. H. Keum, S. Cho, J. H. Kim, D.-H. Choe, H.-J. Sung, M. Kan, H. Kang, J.-Y. Hwang, S. W. Kim, H. Yang, K. J. Chang. and Y. H. Lee, Nat. Phys. **11**, 482 (2015).

[55] T. Zandt, H. Dwelk, C. Janowitz, and R. Manzke, J. Alloys Compd. **442**, 216 (2007).

[56] M. N. Ali, J. Xiong, S. Flynn, J. Tao, Q. D. Gibson, L. M. Schoop, T. Liang, N. Haldolaarachchige, M. Hirschberger, N. P. Ong, and R. J. Cava, Nature (London) **514**, 205 (2014).